2018 Annual American Control Conference (ACC)
June 27–29, 2018. Wisconsin Center, Milwaukee, USA

Intelligent Cruise Control of Diesel Powered Vehicles Addressing the Fuel Consumption Versus Emissions Trade-off

Chunan Huang, Rasoul Salehi and Anna G. Stefanopoulou

Abstract— **Intelligent cruise control with traffic preview introduces a potential to adjust the vehicle velocity and improve fuel consumption and emissions. This paper presents trade-offs observed during velocity trajectory optimizations when the objective function varies from fuel-based targets to emissions-based. The scenarios studied consider velocity optimization while following a hypothetical leader executing the federal test procedure (FTP) velocity profile with distance constraint, instead of the classical legislated velocity constraint, to enable the flexibility in optimizing the velocity trajectory. The vehicle model including longitudinal dynamics, fuel consumption and tailpipe NOx emissions is developed for a medium-duty truck with a diesel engine and verified over the FTP. Then, dynamic programming is applied on a reduced-order model to solve the constraint trajectory optimization problem and calculate an optimal vehicle velocity profile over the temperature stabilized phase (Bag 2) of the FTP. Results show 59% less tailpipe NOx emissions with an emission-optimized drive cycle but with 17% more fuel consumption compared to a non-optimized baseline. Whereas, a fuel-optimized cycle improves the fuel efficiency by 18% but with doubled tailpipe NOx emissions. Moreover, it is shown that for a diesel powertrain, including the aftertreatment system efficiency associated with the thermal dynamics is crucial to optimize the tailpipe NOx emissions and can not be ignored for problem simplification.**

I. INTRODUCTION

Vehicle autonomy, semi-autonomy, or plain driver-advisory velocity signal could assist in reducing emissions and fuel consumption by allowing a flexible speed trajectory to the autonomous vehicle in a given traffic condition. Assuming a hypothetical leader, the follower autonomous vehicle should be able to navigate itself to stay in a distance after the hypothetical leader, ensuring the driver safety and no car cuts in from other lanes. To clarify the benefits and also inform policy makers, the hypothetical lead is scheduled here to transverse the standard FTP-72 drive cycle. Enforcing the distance constraint, the follower's speed profile can be optimized to have minimal acceleration, so that fuel economy is improved indirectly due to removal of acceleration spikes [1]. Other constraints such as trip time [2], road topography [3], traffic conditions [4] and traffic signals [5] can also be included in the fuel optimization to replicate all conditions that happen in real road traffic and travel missions.

Similar to the fuel economy, vehicle emissions are also vehicle velocity dependent and depend on how the autonomous vehicle follows the leader. An aggressive acceleration, for example, generates a peak in the engine out emissions which can challenge the clean-up capability of the vehicle aftertreatment system. With the traffic preview, the vehicle might be driven such that the engine raw emissions are low or/and the aftertreatment system is active enough to keep the tailpipe emissions, such as NOx, within regulations limits. NOx emissions reduction in modern diesel engines heavily relies on a Selective Catalytic Reduction (SCR) aftertreatment system [6] with a configuration shown in Fig. 1. The SCR catalyst uses a reducing agent, ammonia (NH_3), to react with NOx and reduce it to nitrogen and oxygen, and its efficiency is highly dependent on catalyst brick temperature. For example, a Cu/Zeolite based SCR system has more than 95% efficiency in the range [220-320]$^\circ C$, while the efficiency drops to 60% at 150$^\circ C$ and is only 20% at 130$^\circ C$ [7]. Therefore, it is critical to control the aftertreatment temperature as well as the engine raw emissions to reduce the vehicle tailpipe (TP) emissions, both dependent on the driving style.

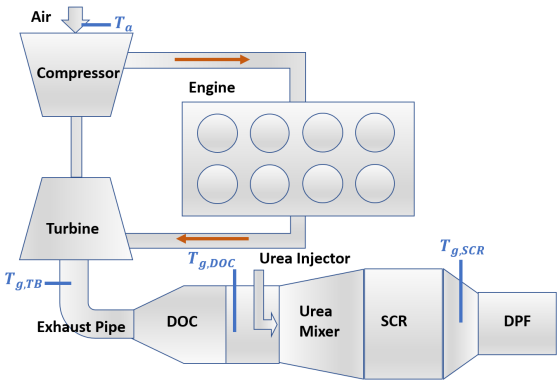

Fig. 1. Aftertreatment system configuration for 6.7L diesel engine considered in this paper

The engine raw emissions reduce inherently when full pedal accelerations are avoided [8], however, tailpipe emissions also depends on the aftertreatment system performance and its control. In-cylinder post fuel injection is a common technique used to increase SCR temperature [9], [10], however, the late injection reduces the vehicle fuel economy. In [11], a coordinated active thermal management is applied to control post-injection and urea injection into SCR for reducing 97.8% of engine out NOx emissions while satisfying NH_3 slip requirements in a known and fixed speed profile. For hybrid electric vehicles, combustion engines and electric motor can be coordinated by the energy management to optimize fuel economy and tailpipe emissions for a given drive cycle by choosing torque split ratio [12], [13]. However,

*This research was supported by National Science Foundation Grant 1646019 with PI Dr. Tulga Ersal and Co-PI Prof. Mingyan Liu.

Chunan Huang, Rasoul Salehi and Anna G. Stefanopoulou are with the Department of Mechanical Engineering, University of Michigan, Ann Arbor, Michigan, 48109, U.S.A. {huangchu,rsalehi,annastef}@umich.edu

in all aforementioned works the aftertreatment system is controlled while the vehicle speed profile is assumed as a fixed trajectory with limited violation boundary permitted by the standard FTP test. In [8], a following distance corridor is considered to optimize speed profile for better fuel economy and diesel engine emissions. Through reducing fast transients of pedal input, their experimental results showed 24% engine NOx reduction with 13% fuel consumption reduction. However, steady state emission or performance of after-treatment was not included.

In this paper, optimal following of a hypothetical leader vehicle is used to study fuel economy-tailpipe NOx emissions trade-offs. The hypothetical lead is scheduled to transverse the standard FTP-72 drive cycle. A following vehicle model is developed to calculate the longitudinal dynamics, engine fuel and raw NOx emissions, and also tailpipe NOx. Optimal speed trajectory for the following vehicle is calculated given different objectives functions including minimum acceleration, minimum fuel consumption, minimum engine NOx emissions and minimum tailpipe NOx. Dynamic Programming (DP) is used to solve the optimization problems constrained by the distance between the two vehicles over the temperature stabilized phase (Bag 2) of the FTP. Results of all optimization scenarios and a baseline vehicle driving the standard drive cycle shows a clear fuel economy-NOx emissions trade-off and indicates the importance of the aftertreatment system in the vehicle trajectory planning.

II. Vehicle Model

A vehicle model for a MY2013 Ford F-350 Super-duty truck with a 6.7L diesel engine is developed to simulate fuel consumption and NOx emission over a drive cycle. The model includes the vehicle longitudinal dynamics, the powertrain steady-state maps and the aftertreatment system thermal dynamics, as shown in Fig. 2. To enable drive cycle design and optimization, vehicle acceleration is considered the main input, then vehicle speed and position, as the states, and the traction force are calculated using the vehicle longitudinal dynamics. A six speed gearbox, similar to the production vehicle, is assumed in the model and the torque converter is simplified to a constant efficiency factor.

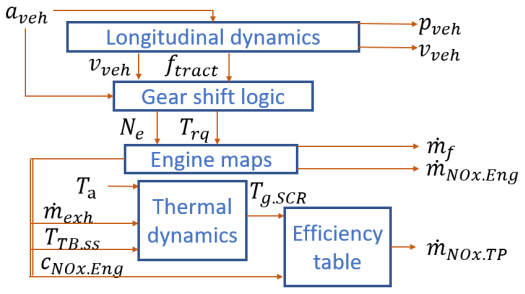

Fig. 2. Schematic of the vehicle model

A. Longitudinal dynamics

The longitudinal dynamics computes vehicle traction force, f_{tract}, given vehicle speed v_{veh} and acceleration a_{veh}:

$$f_{tract} = M_v a_{veh} + f_{rr} + f_{air} \tag{1}$$

$$f_{rr} = C_R M_v g, \text{ if } v_{veh} > 0 \tag{2}$$

$$f_{air} = 0.5 \rho_{air} A_f C_d v_{veh}^2 \tag{3}$$

with f_{rr} the rolling resistance, f_{air} the air drag resistance, M_v vehicle mass, A_f the vehicle frontal area, C_d and ρ_{air} the air drag coefficient and density, and C_R the rolling resistance coefficient. Assuming the vehicle as a point mass system, v_{veh} and the vehicle position p_{veh} are calculated using:

$$\begin{bmatrix} \dot{p}_{veh} \\ \dot{v}_{veh} \end{bmatrix} = \begin{bmatrix} v_{veh} \\ a_{veh} \end{bmatrix}. \tag{4}$$

The gear shift logic is designed to be a function of the vehicle speed and acceleration such that at a given (v_{veh}, a_{veh}) point there is a unique gear level. Further, the transmission efficiency is assumed 75%. The constant parameters in the longitudinal dynamics (1)-(4) are identified using measured vehicle speed, engine speed and torque with validation results shown in Fig. 3. As shown, the model follows engine speed and torque trajectory quite well, except that it predicts more oscillations in both engine speed and torque during transient conditions. One reason for these oscillations is that the model does not include the torque converter, which could damp out the engine speed and torque oscillations.

B. Engine and efficiency models

Fuel rate $\dot{m}_f$, exhaust flow rate $\dot{m}_{exh}$, engine out NOx concentration $c_{NOx.Eng}$ (in ppm) and steady state turbine out temperature $T_{TB.ss}$ are calculated using look-up tables mapped with engine speed N_e and torque T_{rq}:

$$[\dot{m}_f, \dot{m}_{exh}, c_{NOx.Eng}, T_{TB.ss}] = f_{Eng}(N_e, T_{rq}) \tag{5}$$

As Eq. (5) suggests, the engine air path dynamics are ignored. The vehicle NOx emissions are modeled using the following two simplifying assumptions: 1) engine raw NOx contains only NO, and NO oxidization in diesel catalytic converter (DOC) is ignored since DOC temperature is nearly always lower than 250 °C in the stabilized phase [7]. 2) the SCR efficiency η_{SCR} is determined by an efficiency table based on SCR brick temperature $T_{b.SCR}$ [7]. Therefore, tailpipe NOx concentration, $c_{NOx.TP}$ is calculated:

$$c_{NOx.TP} = (1 - \eta_{SCR}) c_{NOx.Eng}. \tag{6}$$

Then, $\dot{m}_{NOx.Eng}$ and $\dot{m}_{NOx.TP}$, which are engine raw emission and tailpipe emission rates, are calculated using NOx concentration and the exhaust flow rate.

C. Aftertreatment system thermal dynamics

The SCR temperature required to calculate η_{SCR} in (6) is calculated by modeling complete aftertreatment system shown in Fig. 1. A first order lag is assumed for turbine outlet gas temperature, $T_{g.TB}$, dynamics:

$$T_{g.TB} = \frac{1}{1 + \tau s} T_{TB.ss} \tag{7}$$

where τ is assumed to be inversely proportional to exhaust mass flow rate, $\tau \propto \frac{1}{\dot{m}_{exh}}$. This accounts for the observation that the faster mass flow rate, the faster could be the $T_{g.TB}$ response.

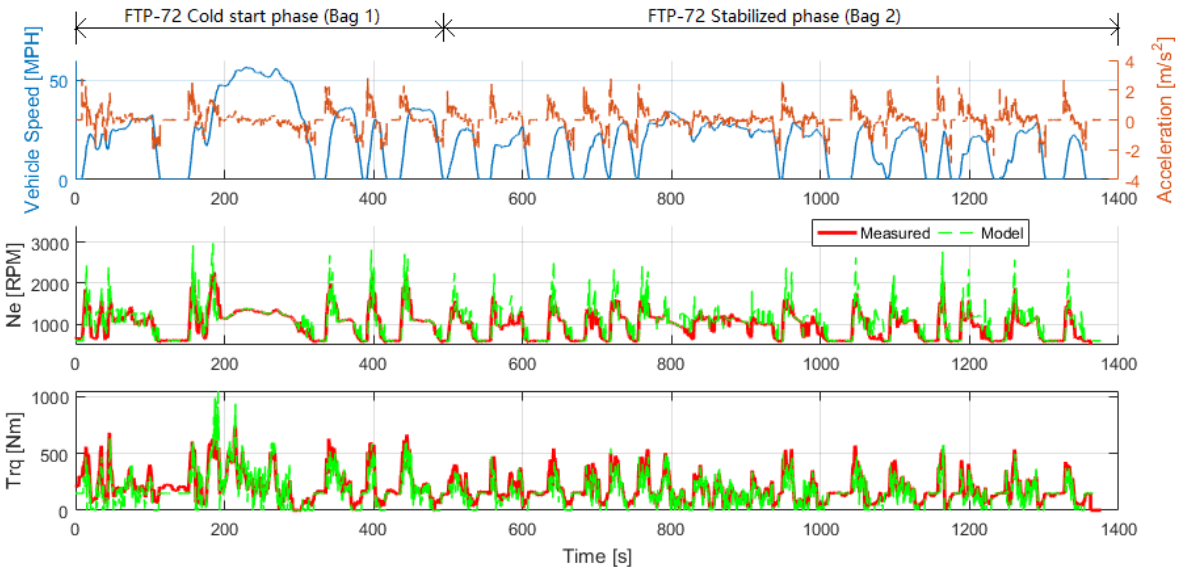

Fig. 3. Validation results for the vehicle longitudinal model

The DOC and SCR catalysts are thermal masses and their thermal models are derived under the following assumptions:

- Heat conduction from the exhaust gas into the catalytic brick is negligible compared with heat convection between them.
- Axial heat diffusion in the fluid phase and axial conduction in the solid phase are ignored.
- Heat capacity of the gas trapped in the catalytic brick is too small compared with that of the brick. So there is no dynamics for the gas temperature inside the catalyst.
- Heat radiations between the gas and the brick, and between the brick and the ambient are ignored.

With these assumptions, a first-order system is proposed to model the thermal dynamics of the DOC [14].

$$T_{g.DOC} = \frac{\frac{\dot{m}_{exh}C_{pg}}{(A\Delta x)_{DOC}} T_{in_{delay}.DOC} + (h_1a_1)_{DOC} T_{b.DOC}}{(h_1a_1)_{DOC} + \frac{\dot{m}_{exh}C_{pg}}{(A\Delta x)_{DOC}}} \tag{8}$$

$$(1-\varepsilon_{DOC})\rho_b C_b \frac{dT_{b.DOC}}{dt} = (h_1a_1)_{DOC}(T_{g.DOC} - T_{b.DOC}) - (h_2a_2)_{DOC}(T_{b.DOC} - T_a) \tag{9}$$

where $T_{g.DOC}$ and $T_{b.DOC}$ are the DOC outlet gas and brick temperatures, T_a is the ambient temperature, A and Δx are the frontal area and length of the brick, C_{pg} and C_b are the specific heat capacities of the exhaust gas and monolith, ρ_b is the density of the monolith, ε_{DOC} is a parameter showing the fraction of the DOC open cross sectional area [15], h_1 and h_2 are the heat convection coefficient from the gas flow to the monolith, and from the block surface to the ambient, a_1 and a_2, are the corresponding geometric surface area-to-volume ratios [15].

$T_{in_{delay}.DOC}$ in (8) is calculated as:

$$T_{in_{delay}.DOC}(t) = T_{g.TB}(t - \Delta\tau_{d.DOC}) \tag{10}$$

$$\int_{t-\Delta\tau_{d.DOC}}^{t} \dot{m}_{exh} ds = l_{d.DOC} \tag{11}$$

$\Delta\tau_{d.DOC}$ is a delay time which is defined to account for a residence time needed for heat to propagate into the monolith [14], and it causes a dead-time in DOC temperature when engine operation condition changes. $l_{d.DOC}$ is a constant parameter proportional to the distance which heat propagate in the DOC brick. To calculate the heat convection, h_1a_1 and h_2a_2 are assumed to be a linear function of $\dot{m}_{exh}$:

$$(h_ia_i)_{DOC} = \alpha_i \dot{m}_{exh} + \beta_i,\ i = 1,2 \tag{12}$$

where α_1, α_2, β_1 and β_2 are constant parameters to be identified. As shown in (8) and (9), the presented thermal model ignores exothermic reactions of CO and unburned hydrocarbons with oxygen in the DOC, which happens mainly when there is in-cylinder post injection.

The same model structure is considered to calculate the SCR output gas ($T_{g.SCR}$) and brick temperature ($T_{b.SCR}$) because of the similar physical structures of SCR and DOC.

$$T_{g.SCR} = \frac{\frac{\dot{m}_{exh}C_{pg}}{(A\Delta x)_{SCR}} T_{in_{delay}.SCR} + (h_1a_1)_{SCR} T_{b.SCR}}{(h_1a_1)_{SCR} + \frac{\dot{m}_{exh}C_{pg}}{(A\Delta x)_{SCR}}} \tag{13}$$

$$(1-\varepsilon_{SCR})\rho_b C_b \frac{dT_{b.SCR}}{dt} = (h_1a_1)_{SCR}(T_{g.SCR} - T_{b.SCR}) - (h_2a_2)_{SCR}(T_{b.SCR} - T_a) \tag{14}$$

$$T_{in_{delay}.SCR}(t) = T_{g.DOC}(t - \Delta\tau_{d.SCR}) \tag{15}$$

$\tau_{d.SCR}$ is calculated using a similar equation as (11) with different parameters identified for SCR. Furthermore, based on simulation results, the change of $\dot{m}_{exh}$ and T_{in} caused by urea solution injection is found to be small and therefore are ignored in the SCR model.

Figure 4 shows the validation results of the aftertreatment system gas temperatures compared with real vehicle measurements. Due to the delayed structure of the thermal dynamics presented in (7)-(15), temperature histories from the cold start phase are required as initial conditions in

the DOC and SCR models in the stabilized phase. Thus, in all temperature calculations in this paper, simulations start from the cold start phase to provide reasonable initial condition for the stabilized phase, but only the stabilized phase is used for comparison and verification. As observed, the gas temperature dynamics is effectively slowed down from $T_{g.TB}$ to $T_{g.SCR}$. The thermal model sometimes misses the dynamics in Bag 1 as it does not include post-injection or water condensation effect. The dynamics in Bag 2, however, is captured well and this is the period considered in the optimization section.

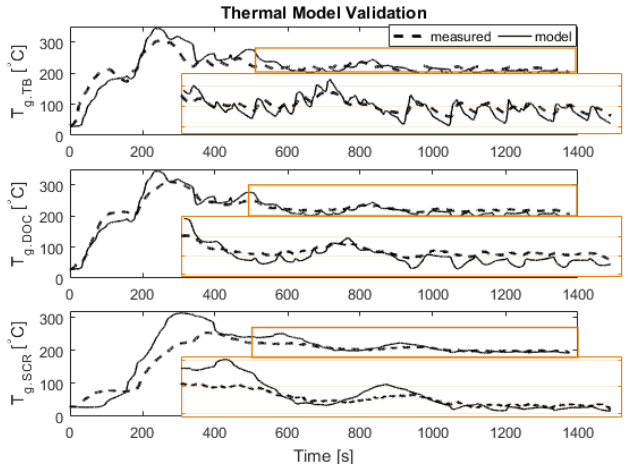

Fig. 4. Thermal model validated over the standard FTP drive cycle

III. Optimization

The speed trajectory of the autonomous vehicle is optimized when it is following a hypothetical leader vehicle driving the standard FTP drive cycle. The optimization minimized one of these four objectives: acceleration, fuel consumption, engine raw NOx emission and tailpipe emission. The following vehicle is designed to drive exactly the FTP cycle during the cold start phase in all optimization cases where post injection and other warm up control strategies are active. Thus, the speed optimization only considers the second phase of the FTP. To simulate real traffic conditions, upper and lower limits of the following vehicle position are defined based on the leader vehicle position and speed, and used as a constraint in the optimization.

The dynamic programming function from MATLAB [16] is used to solve the speed trajectory optimization problem. Since including all the states in vehicle longitudinal model and thermal model will lead to a huge computation burden, instead of the thermal model described in section II-C, a reduced-order model with only one state is used in DP to simulate SCR temperature. In the reduced-order model, the aftertreatment system including SCR is assumed to be lumped to a thermal mass with the following dynamics:

$$T_{g.rSCR} = \frac{\frac{\dot{m}_{exh}C_{pg}}{(A\Delta x)_{rSCR}}T_{TB.ss} + (h_1a_1)_{rSCR}T_{b.rSCR}}{(h_1a_1)_{rSCR} + \frac{\dot{m}_{exh}C_{pg}}{(A\Delta x)_{rSCR}}} \tag{16}$$

$$\begin{aligned}(1-\varepsilon_{rSCR})\rho_b C_b \frac{dT_{b.rSCR}}{dt} &= (h_1a_1)_{rSCR}(T_{g.rSCR} - T_{b.rSCR}) \\ &\quad - (h_2a_2)_{rSCR}(T_{b.rSCR} - T_a)\end{aligned} \tag{17}$$

where $T_{g.rSCR}$ and $T_{b.rSCR}$ represent outlet gas and brick temperature for the SCR reduced model. Compared with the original model, the reduced lumped model has only one state (instead of three) and the delay terms in (10) and (15) are ignored.

Four optimization scenarios are tested with a single objective function in each case as:

$$J_i(x) = \min_{\{a_{veh}(k)\}_{k=0}^{N}} \sum_{k=0}^{N} C_i(k), \quad i = 1,2,3,4 \tag{18}$$

subject to

$$-6 \text{ m/s}^2 \le a_{veh}(k) \le 6 \text{ m/s}^2 \tag{19}$$

$$\underline{p}(v_l(k)) \le p_{veh}(k) \le \bar{p}(v_l(k)) \tag{20a}$$

$$\bar{p}(v_l(k)) = p_l - v_l \cdot \Delta t_L \tag{20b}$$

$$\underline{p}(v_l(k)) = p_l - \begin{cases} v_l d_{max} & \text{if } v_l < 20 \text{ MPH} \\ v_l d_{min} & \text{otherwise} \end{cases} \tag{20c}$$

$$0 \le v_{veh}(k) \le 67 \text{ MPH} \tag{21}$$

$$150^\circ C \le T_{b.rSCR}(k) \le 300^\circ C \tag{22}$$

and system dynamics (1-7,16,17) discretized using $dT = 0.1s$, with a zero-order hold on input u. In above, $k = 0$, N represents the starting step and ending step of the stabilized phase in FTP, p_l and v_l are the position and velocity of the leader vehicle, Δt_L is selected proportional to the vehicle length, d_{max} and d_{min} are selected 10ft/MPH and 4ft/MPH. $\bar{p}(v_l(k))$ is the closest position of follower car considered for safety and $\underline{p}(v_l(k))$ is the farthest position that would prevent cut-ins from other lines [1]. Table I describes the cost function used in each optimization scenario and its corresponding states.

TABLE I

Cost functions defined for optimization scenarios

Objective	Cost function	States
(optimal) acceleration	$C_1(k) = a_{veh}(k)^2$	$[p_{veh}, v_{veh}]^T$
(optimal) fuel or MPG	$C_2(k) = m_f(k)$	$[p_{veh}, v_{veh}]^T$
(optimal) Engine NOx	$C_3(k) = m_{NOx.Eng}(k)$	$[p_{veh}, v_{veh}]^T$
(optimal) TP NOx	$C_4(k) = m_{NOx.TP}(k)$	$[p_{veh}, v_{veh}, T_{b.rSCR}]^T$

Finally, inputs and states are discretized before applying DP with grid sizes

$$\Delta a_{veh} = 0.5 \text{ m/s}^2, \quad \begin{cases} \Delta p_{veh} = \frac{\bar{p}(v_l(k)) - \underline{p}(v_l(k))}{30} \text{ m} \\ \Delta v_{veh} = \frac{1}{4} \text{ m/s} \\ \Delta T_{b.rSCR} = 3^\circ C \ . \end{cases} \tag{23}$$

IV. Results

The following autonomous vehicle is simulated with the optimized speed profile for each of the four scenarios listed in Table I. Main results for the two extreme cases, namely least fuel and least TP emissions, are shown in Fig. 5. Detailed key results including the vehicle fuel economy (in MPG), engine raw emissions, NOx reduction rate, and tailpipe emissions are listed in Table II for all four cases.

As plotted in Fig. 5, MPG in fuel optimized scenario is 18% higher than the standard baseline, but tailpipe NOx is almost doubled; while directly optimizing tailpipe emission decreases NOx 59% compared to the standard with 17% less fuel efficiency. Therefore, a complete trade-off exists between the vehicle fuel economy and emissions such that improving one deteriorates another.

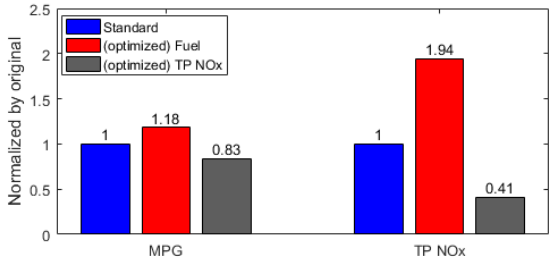

Fig. 5. Summary of the fuel & TP NOx optimization results normalized by the standard FTP drive cycle

Speed trajectories for the four scenarios in Table I and the standard driving are shown in Fig. 6. As shown, all four optimization scenarios recommend a relatively constant speed over [690-710]s. When the fuel is minimized, a pulse and glide speed trajectory is generated. This commands the engine to operate with high torque as is shown in visitation plot in Fig. 8-(d). The engine, however, generates very high amount of NOx at high torque conditions, specifically if the engine speed is low (Fig. 8-(b)). This is the reason that raw emissions increased with fuel optimized drive cycle as shown in Table II.

TABLE II

EFFECT OF OPTIMIZATION OBJECTIVE ON MAJOR VEHICLE OUTPUTS

Objective	Orig.	Acce.	Fuel	Eng. NOx	TP NOx
MPG	16.3	18.2	19.3	19.2	13.7
Engine NOx [g]	5.20	3.50	8.09	3.24	5.47
Tailpipe NOx [g]	0.342	0.388	0.664	0.385	0.141
NOx reduction [%]	93.4	88.9	91.8	88.1	97.4
Urea Solution [g]	14.2	9.10	21.7	8.33	15.6

SCR temperature traces for all five cases are shown in Fig. 7 along with 97.5%, 95% and 85% SCR efficiency levels. As observed, the SCR temperature and consequently its efficiency is low when only the fuel economy is optimized. The low SCR efficiency together with the high raw engine emissions are reasons that the tailpipe NOx is doubled compared to the standard FTP driven speed profile as Table II shows. From Fig. 7 it is observed that maintaining high temperature for the SCR is required to minimize the tailpipe NOx emissions. To increase the SCR temperature, DP designs the vehicle speed such that the turbine out temperature rises as verified by $T_{TB.ss}$ distribution shown in Fig. 9. The cost for this high SCR temperature, however, is higher fuel consumption since the high $T_{TB.ss}$ points are not necessarily located in high engine efficiency regions.

Finally, results from the acceleration and engine NOx minimized optimizations are found to be between the fuel and the tailpipe emission minimized scenarios (Table II). Therefore, the two former objective functions can be used to compromise between fuel and tailpipe emissions. Especially, the raw emissions minimization scenario is recommended since it improves fuel economy while maintains tailpipe emission level close to the baseline speed profile.

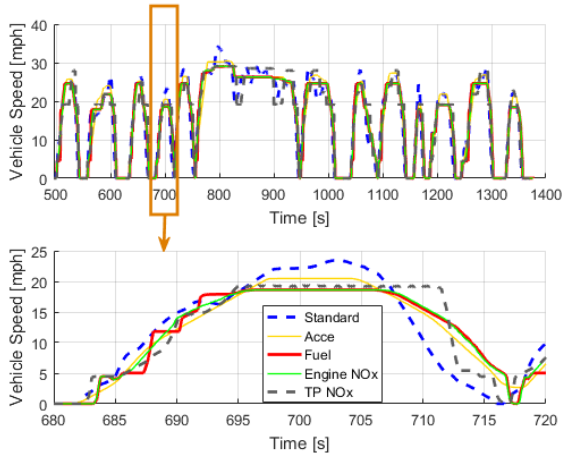

Fig. 6. Comparison between the standard and optimized vehicle speed trajectories

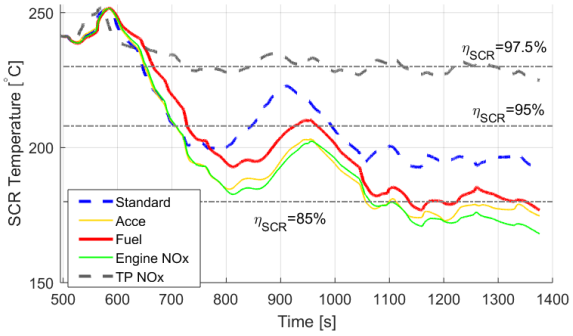

Fig. 7. SCR temperature for the various optimization objectives

V. CONCLUSIONS

Vehicle speed trajectory optimization scenarios were tested to minimize four objective functions, namely acceleration, fuel consumption, engine NOx emissions, and tailpipe NOx emissions. A model was developed for a medium duty diesel truck to calculate fuel consumption and NOx emissions. The vehicle followed a hypothetical leader which was driven based on the standard FTP drive cycle. Then, dynamic programming was applied to calculate optimal velocity trajectory for the following vehicle during the stabilized (warmed-up) phase of the FTP.

Results showed when only the fuel economy was optimized, the tailpipe NOx emissions were doubled (compared to a non-optimized baseline) due to low aftertreatment efficiency and high engine emissions. When the optimization target was changed to the tailpipe emissions, however, 17% of the fuel efficiency was sacrificed to keep the aftertreatment efficiency high, which lowered down tailpipe NOx emissions by 59%. Therefore, it was concluded that maximum fuel saving from an autonomous driving cannot be achieved at the same time the maximum emission reduction is reached. Finally, it is observed that minimizing the engine out emissions would not reduce tailpipe emissions and one should include the aftertreatment system thermal dynamics in the optimization problem. As a future work, it is recommended to

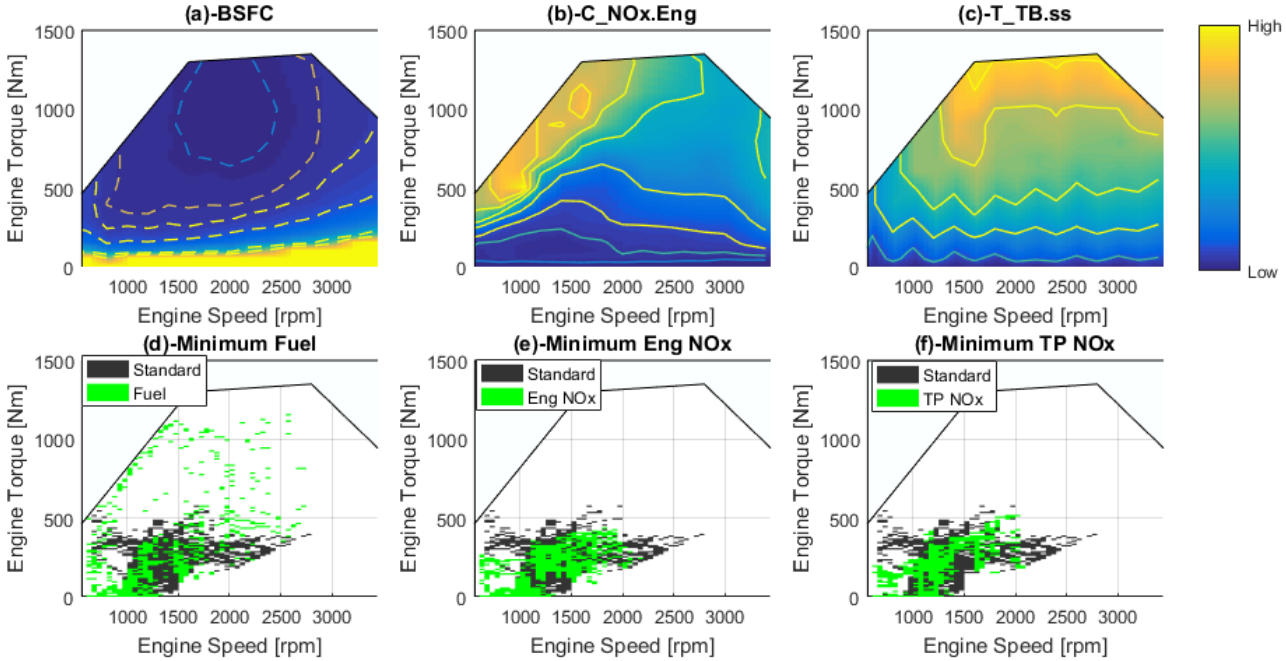

Fig. 8. Engine maps for BSFC, $C_{NOx.Eng}$, $T_{TB.ss}$, and visitation points from different optimization scenarios compared with the standard FTP drive cycle

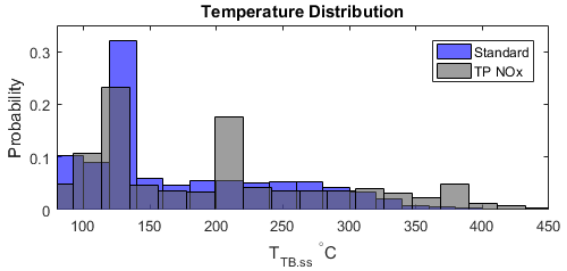

Fig. 9. $T_{TB.ss}$ probability distribution comparison between tailpipe NOx optimization scenario and the standard FTP drive cycle

formulate a fuel and tailpipe NOx emissions co-optimization problem and solve it to calculate the vehicle speed trajectory using a causal methodology such as the model predictive control.

ACKNOWLEDGMENT

The authors would like to thank Michiel Van Nieuwstadt and Cory Hendrickson from Ford Research and Advanced Engineering for providing valuable data and suggestions regarding constructing the model.

REFERENCES

[1] N. Prakash, G. Cimini, A. G. Stefanopoulou, and M. J. Brusstar, "Assessing fuel economy from automated driving: Influence of preview and velocity constraints," in *ASME 2016 Dynamic Systems and Control Conference*. American Society of Mechanical Engineers, 2016, pp. V002T19A001–V002T19A001.

[2] F. Mensing, E. Bideaux, R. Trigui, and H. Tattegrain, "Trajectory optimization for eco-driving taking into account traffic constraints," *Transportation Research Part D: Transport and Environment*, vol. 18, pp. 55–61, 2013.

[3] V. Turri, B. Besselink, J. Mårtensson, and K. H. Johansson, "Fuel-efficient heavy-duty vehicle platooning by look-ahead control," in *Decision and Control (CDC), 2014 IEEE 53rd Annual Conference on*. IEEE, 2014, pp. 654–660.

[4] C. R. He, H. Maurer, and G. Orosz, "Fuel consumption optimization of heavy-duty vehicles with grade, wind, and traffic information," *Journal of Computational and Nonlinear Dynamics*, vol. 11, no. 6, p. 061011, 2016.

[5] M. A. S. Kamal, M. Mukai, J. Murata, and T. Kawabe, "Model predictive control of vehicles on urban roads for improved fuel economy," *IEEE Transactions on Control Systems Technology*, vol. 21, no. 3, pp. 831–841, May 2013.

[6] G. D. Neely, S. Sasaki, Y. Huang, J. A. Leet, and D. W. Stewart, "New diesel emission control strategy to meet US Tier 2 emissions regulations," SAE, Warrendale, PA, Tech. Rep. 2005-01-1091, 2005.

[7] G. Cavataio, H.-W. Jen, J. R. Warner, J. W. Girard, J. Y. Kim, and C. K. Lambert, "Enhanced durability of a Cu/zeolite based SCR catalyst," *SAE International Journal of Fuels and Lubricants*, vol. 1, no. 2008-01-1025, pp. 477–487, 2008.

[8] R. Schmied, H. Waschl, R. Quirynen, M. Diehl, and L. del Re, "Nonlinear MPC for emission efficient cooperative adaptive cruise control," *IFAC-PapersOnLine*, vol. 48, no. 23, pp. 160–165, 2015.

[9] J. Parks, S. Huff, M. Kass, and J. Storey, "Characterization of in-cylinder techniques for thermal management of diesel aftertreatment," SAE, Warrendale, PA, Tech. Rep. 2007-01-3997, 2007.

[10] O. Lepreux, Y. Creff, and N. Petit, "Model-based temperature control of a diesel oxidation catalyst," *Journal of Process Control*, vol. 22, no. 1, pp. 41–50, 2012.

[11] P. Chen and J. Wang, "Coordinated active thermal management and selective catalytic reduction control for simultaneous fuel economy improvement and emissions reduction during low-temperature operations," *Journal of Dynamic Systems, Measurement, and Control*, vol. 137, no. 12, p. 121001, 2015.

[12] F. Tschopp, T. Nüesch, M. Wang, and C. Onder, "Optimal energy and emission management of a diesel hybrid electric vehicle equipped with a selective catalytic reduction system," SAE, Warrendale, PA, Tech. Rep. 2015-24-2548, 2015.

[13] D. Kum, H. Peng, and N. K. Bucknor, "Optimal energy and catalyst temperature management of plug-in hybrid electric vehicles for minimum fuel consumption and tail-pipe emissions," *IEEE Transactions on Control Systems Technology*, vol. 21, no. 1, pp. 14–26, 2013.

[14] O. Lepreux, Y. Creff, and N. Petit, "Model-based control design of a diesel oxidation catalyst," *IFAC Proceedings Volumes*, vol. 42, no. 11, pp. 279–284, 2009.

[15] V. Pandey, B. Jeanneret, S. Gillet, A. Keromnes, and L. Le Moyne, "A simplified thermal model for the three way catalytic converter," in *TAP 2016, 21st International Transport and Air Pollution Conference*, 2016, p. 6 p.

[16] O. Sundstrom and L. Guzzella, "A generic dynamic programming matlab function," in *Control Applications,(CCA) & Intelligent Control,(ISIC)*, 2009, pp. 1625–1630.